Faraday Discussions

Elucidating how trace gases interact with ice surfaces utilizing sum frequency generation

Journal:	*Faraday Discussions*
Manuscript ID	FD-ART-10-2024-000157.R2
Article Type:	Paper
Date Submitted by the Author:	29-Nov-2024
Complete List of Authors:	Yettapu, Gurivi Reddy; Boise State University, Department of Chemistry Manning, Luca; Boise State University, Department of Chemistry Cyran, Jenée; Boise State University, Department of Chemistry

ARTICLE

Elucidating how trace gases interact with ice surfaces utilizing sum frequency generation spectroscopy

Received 00th January 20xx,
Accepted 00th January 20xx

DOI: 10.1039/x0xx00000x

Gurivi Reddy Yettapu, [a,†] Luca B. Manning [a,†] and Jenée D. Cyran [a]

The interaction between ice surfaces and trace gases plays a significant role in atmospheric chemistry, such as chemical and photochemical reactions contributing to ozone depletion and secondary aerosol formation. The study of molecular-level properties of the ice surface and small organic molecule adsorption are essential to understand the impact of hosting these molecules and further chemical reactions. To capture a molecular understanding of the interface, the use of a surface selective technique, such as sum frequency generation (SFG) spectroscopy, is crucial to probe ice surfaces and observe the adsorption of molecules on ice surfaces. We observe significant differences in the structure of the water molecules for ice and water surfaces upon the addition of acetone and methanol. At the methanol-ice interface, a blue shift of ~80 cm^{-1} is observed, indicating a weakening of the hydrogen bond. This is an opposing shift to the acetone-ice interface, which red shifted by ~10 cm^{-1}. These changes in the fundamental frequencies could impact atmospheric models and in particular impact overtone pumping reactions. The distinct behavior of water molecules and small oxygenated organic compounds is linked to differences in reactivity and rates of photochemical reactions via overtone pumping on ice and water surfaces.

Introduction

Sunlight driven excitation of overtone transitions of the OH stretching vibration contributes to radical formation of atmospherically relevant species. This mechanism is known as overtone dissociation or vibrational overtone pumping. In 1997, Donaldson et al.[1] proposed an atmospheric mechanism that compounds, such as HNO_3 and HNO_4, could photodissociate from visible excitation of OH overtone vibrations. This mechanism was derived in part from previous spectroscopic results of vibrationally mediated photodissociation of hydrogen peroxide and nitric acid.[2,3] Moreover, the vibrationally mediated photodissociation enhances the OH fragments by three times compared to single photon photolysis.[3] These results provide significant implications for atmospheric processing of OH radicals and thus understanding the structure and vibrational spectra of small atmospherically relevant compounds is essential.

Understanding how atmospheric trace gases interact with ice surfaces is essential for enhancing our knowledge of atmospheric chemistry and its wider environmental impacts. Small organic molecules, such as methanol and acetone, are commonly found in the atmosphere, particularly at low temperatures, where they engage in significant interactions with ice surfaces. These interactions influence processes, such as scavenging of semi-volatile gases by cirrus clouds and the deposition of organic pollutants in snow and sea ice.[4,5] Furthermore, trace gases that adsorb onto ice surfaces can trigger chemical and photochemical reactions that are critical to the chemistry of the ozone layer.[6–9]

Trace gases interacting with water and ice have been studied extensively with mass spectrometry[10–14] and X-ray absorption spectroscopy.[15,16] Mass spectrometry studies dominate the field and focus on quantifying the adsorption isotherms of gas phase molecules on ice and water surface.[17,18] However, these studies do not elucidate the structure of the organic molecules on the surface, which can directly affect the chemical and physical properties of the aqueous interfaces. Infrared spectroscopy, such as reflection-absorption infrared spectroscopy (RAIRS), has been utilized to understand the adsorption and embedding of acetone on ice surfaces.[19] To elucidate vibrational overtone pumping pathways, it is crucial to measure the vibrational spectra of trace gases interacting with ice surfaces.

Sum-frequency generation spectroscopy (SFG) has been a valuable tool in determining the molecular structure and orientation of water molecules at ice-air and water-air interfaces.[20–25] Inversion-symmetry breakdown at interfaces makes SFG a powerful technique to probe the depth of surfaces to angstrom (Å) molecular level.[26,27] In SFG, an infrared beam is in resonance with molecular vibrational mode and visible beam is upconverted to produce SFG light, which in turn reveals the molecular structure of interfacial molecules. The structure and adsorption of methanol and acetone on water surfaces have previously been studied.[28–31] Herein, we employed SFG spectroscopy to directly probe the adsorption of methanol and acetone on water and single crystalline ice surfaces. We probe the adsorption of acetone and methanol by monitoring the CH vibrational modes of these trace gases as well as the impact to the structure of ice and water via the OH modes of water molecules.

Experimental Methods

[a] Boise State University, Department of Chemistry and Biochemistry, 1910 University Drive, Boise, Idaho, 83702, USA.
[b] † Shared first co-authorship.
[c] Supplementary Information available: [details of any supplementary information available should be included here]. See DOI: 10.1039/x0xx00000x

2.1 Materials

Acetone (≥99.5%, HPLC grade) was acquired from VWR Chemicals BDH. Methanol (Laboratory Grade) was received from Fisher Scientific. Nanopore water (Resistivity 18.2 M Ω●cm) was used for ice growth and the liquid samples.

2.2 Single Crystalline Ice Sample Preparation

Single-crystalline hexagonal ice (Ih) was grown using a seed extraction technique from a nanopore water bath, also known as a modified Czochralski method. A hexagonal ice was attached to a temperature-controlled copper pin, regulated by a Peltier and mounted on a motorized stage (ThorLabs LTS300). The seed was fixed to the pin by warming the pin to 1 °C then cooling the pin to below 0 °C while pressed against the seed. A quasi-liquid layer was formed on the ice seed by briefly applying heat with a heat gun, followed by the removal of excess water using clean, pressurized air. The copper pin, with the seed attached, was then lowered until the seed was partially submerged in a nanopore water bath maintained at 0.5 °C by a chiller (Julabo P250). After 1 hour, the extraction process from the nanopore water bath was initiated at a controlled rate of (1.3 mm/h). The seed is grown from the melt for a total of 24 hours, including the initial hour. Remove the finished boule. A Rigsby stage was used to check the crystallinity of the sample, and Formvar etching was used to check the orientation. All ice samples are oriented to the basal plane.

A custom-built ice flow cell was used for SFG experiments on ice surfaces and has been described in detail elsewhere.[32] All components of the ice flow cell were cleaned by submerging the parts in acetone, ethanol, and nanopure water, respectively, and sonicating for 10 minutes each. The components were then dried with clean air and placed in foil on a hot plate at 50 °C overnight (or at least 5 hours) to further dry and evaporate solvents from the sample cell. Once the drying process was complete, the bottom 5 pieces (copper base plate, base Teflon ring, temperature probe holder, o-ring, Teflon screw) were assembled. A boule of single crystalline ice that had been verified for proper crystallinity and orientation was utilized. A slice (~4-6 mm) of single crystalline ice was cut and a sample was prepared using an aluminum circular cutter (44 mm diameter). The cell was placed in the freezer and allowed to cool to 16 °C. Subsequently, the ice sample was placed on the center of the copper pin in the sample cell. The ice sample was microtomed using a clean blade (Leica Surgipath) until the ice sample is 4 mm thick. The sample cell was sealed with a CaF_2 window on top and annealed overnight in a freezer at -20 °C.

2.3 Sum Frequency Generation (SFG) Spectroscopy

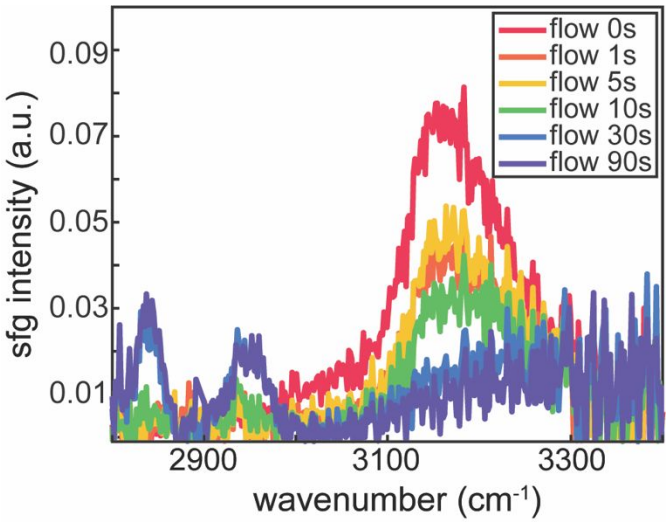

Figure 1. SFG spectra of methanol adsorbed onto the basal plane of the ice surface. Flow 0s corresponds to a flow of only nitrogen gas over the ice surface.

In this work, SFG experiments were conducted with a Ti:Sapphire regenerative amplifier, which generates 800 nm pulses with a pulse duration of 60 fs and a repetition rate of 1 kHz (Astrella, Coherent). A portion of the output is passed through an etalon to generate a narrowband (~10 cm^{-1} FWHM) visible (VIS) pulse, which provides the spectral resolution of the SFG experiments. Another portion of the 800 nm light is used to pump an optical parametric amplifier with a difference frequency generation stage to generate a broad IR pulse (TOPAS-Prime, Light Conversion). The VIS and IR beams are focused onto the sample surface with a 30 cm and 10 cm focusing lens, respectively. The IR and VIS beams are overlapped at the sample with incident angles of 35° and 60°, respectively, with respect to surface normal. SFG signal is generated, collimated and detected on a spectrometer with a grating (1200 grooves/nm) and a charge-coupled device (CCD) camera (ISOPlane 160 and Pixis400, Princeton Instruments). The polarization of both the IR and VIS beams can be controlled by a combination of halfwave plates and polarizers. All SFG spectra shown here were collected in the *ssp* polarization (*s*-polarized SFG, *s*-polarized VIS and *p*-polarized IR). The SFG spectra were background subtracted, where the IR beam was blocked, and are normalized utilizing the non-resonant signal from a z-cut quartz crystal.

For SFG experiments on ice surfaces, the ice cell was placed on the stage, which was cooled to -50 °C using a chiller (Julabo 1000F). A temperature sensor is placed into the cell to monitor the temperature. The ice sample cell was moved in an offset circular motion in order to mitigate melting the sample, as previously described. Cool the stage by gradually increasing the voltage to the Peltier, ensuring that the cooling rate of the ice does not exceed 10 °C per 10 minutes to prevent cracking. Nitrogen was used as a carrier gas for flow experiments. The flow rate for all experiments was 2 L/hr. To flow acetone or methanol onto the ice surface a bubbler containing 300 uL of solvent was added to the inlet. The flow was stopped after the exposure times indicated in Figure 1 and the SFG spectra were collected. The acquisition times were 1 minute for the spectral region from 2800 to 3400 cm^{-1} and were 10 minutes for the

spectral region from 3400 to 3800 cm^{-1}. Five spectra were averaged for each of the time points to obtain the spectra illustrated in Figure 1.

For SFG experiments on methanol and acetone in aqueous solutions, the samples were cooled to ~0 °C. The sample cell for the liquid experiments was the same as for the ice experiments except for a small Teflon dish inside the cell. The sample cell was closed with a CaF_2 window and a threaded lid to limit evaporation. The spectra were acquired for 10 minutes in both spectral regions, from 2800 to 3400 cm^{-1} (hydrogen bonded and CH region) and from 3400 to 3800 cm^{-1} (free OH region).

Results and discussion

lower wavenumber as methanol was vapor deposited on the surface, indicating methanol molecules are being adsorbed on to the ice surface. The intensity of these peaks increases with flow time indicates a greater number of methanol molecules on the surface. The most prominent peak arises at ~2840 cm^{-1} is assigned to the C-H symmetric stretching of methyl group in the methanol. The second most intense peak at ~2944 cm^{-1} and shoulder peak on its lower energy side at ~2920 cm^{-1} arise from Fermi resonance (FR) splitting of symmetric stretching mode of C-H bond with its overtone bending mode. After roughly 30s of flowing methanol onto the ice surface, there is a significant decrease in the O-H signal from the ice surface. The O-H signal from the ice surface with the adsorption of acetone

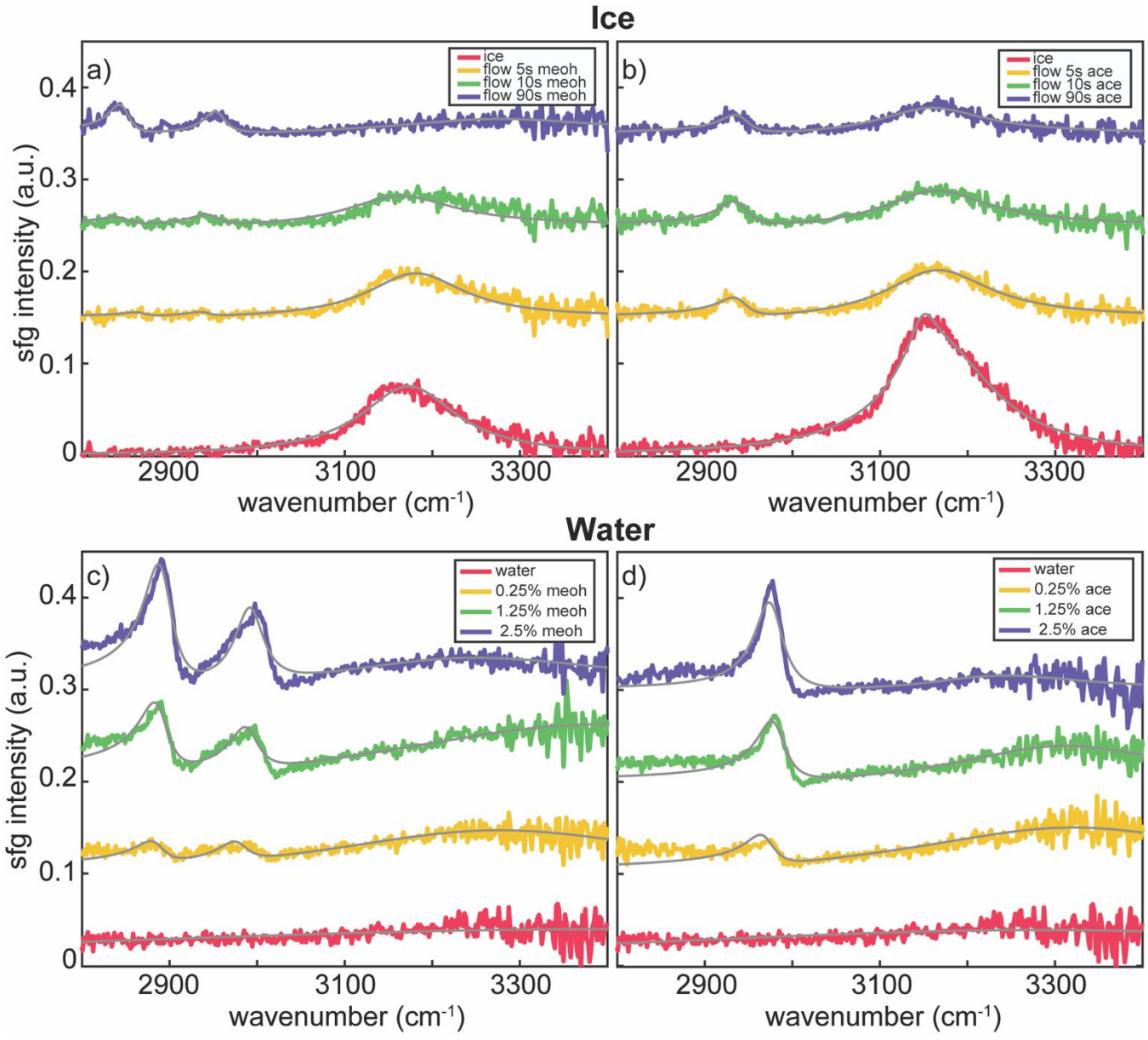

Figure 2. SFG spectra of a) methanol on ice surface, b) acetone on ice surface, c) methanol on water surface, and d) acetone on water surface. The spectral fits, following equation 1, to the data are in grey.

The experimental SFG spectra of methanol-ice interfaces are shown in Figure 1. The ice-air interface has one spectral feature at ~3170 cm^{-1} for the hydrogen bonded O-H vibration in the spectral region from 2800 to 3400 cm^{-1}. We observed additional features at

also decreases but to a lesser extent.

To understand quantitatively these effects, we fitted the SFG spectra obtained on both the interfaces with the Lorentzian oscillator model given by

$$I_{SFG} = \left| A_{NR} e^{i\varphi_{NR}} + \sum_n \frac{A_n}{\omega_{IR} - \omega_n + i\Gamma_n} \right|^2 \quad (1)$$

Where $A_{NR}e^{i\varphi_{NR}}$ is the non-resonant (NR) contribution; A_{NR} and φ_{NR} are amplitude and phase of the NR contribution, respectively, and were held at zero for all fits. A_n is the strength of the vibrational mode, n, ω_{IR} is central frequency of the resonance, and Γ_n is the linewidth of the resonance, n.

Representative SFG spectra for methanol and acetone adsorbed onto ice and water surfaces are illustrated in Figure 2. The grey lines are fits to the experimental data. At the pure ice/air and water/air surfaces, the spectra contain signals from the bonded O-H stretch vibrations at ~3170 cm^{-1} and 3250 and 3400 cm^{-1}, respectively. As methanol and acetone are added to the surfaces, spectral features corresponding to the C-H vibrations arise in the SFG spectra. For acetone, the CH region has one spectral feature corresponding to the C-H symmetric stretch vibration at ~2940 cm^{-1}.

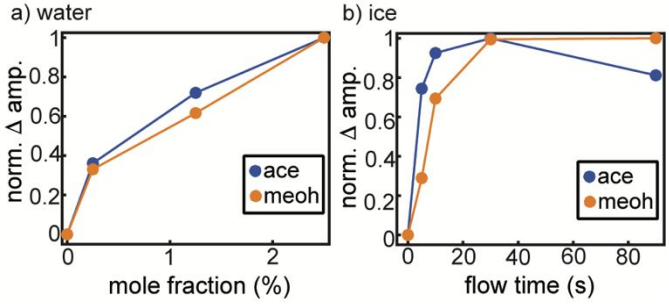

Figure 3. Extracted amplitudes of the CH vibrations for acetone and methanol on a) water surfaces and b) ice surfaces. For methanol, the 2944 cm^{-1} peak was used for analysis. However, the trends remain the same with the CH peak at 2840 cm^{-1}.

The normalized change in amplitudes (arbitrary units) of the C-H vibrations from the fits are illustrated in Figure 3. Here, the amplitudes were extracted from the fits at ~2944 cm^{-1} for methanol and ~2940 cm^{-1} for acetone and the change in the amplitudes was normalized to generate Figure 3. For both ice and water interfaces, the C-H amplitudes of acetone and methanol increase with small concentrations. For methanol and acetone on ice surfaces, the C-H signal reaches a maximum at ~30 s, which may indicate a monolayer at the surface. For the liquid samples, the C-H signal continues to increase at the low concentrations studied here. Previous results have shown that a decrease in C-H signals occur at much higher concentrations of acetone and methanol on water surfaces.[28,29] Moreover, the decrease in C-H signal at higher concentrations at aqueous interfaces has been studied and reveals a formation of bilayers of methanol and acetone at the aqueous interface. Based on our results and previous literature, the maximum intensity is where you form a monolayer on the ice and water surface with methanol and acetone. After the maximum is reached, bilayers begin to form.

A previous study has measured the adsorption isotherms of acetone and methanol on ice surfaces utilizing mass spectrometry. The adsorption isotherms were used to derive the enthalpy of adsorption, which was found to be more favourable for methanol compared to acetone.[13] Based on our SFG spectroscopy results, the adsorption isotherms of acetone and methanol would be within the error of the measurements. Therefore, based on the current data, we only use the C-H amplitudes to indicate a relative surface coverage of acetone and methanol molecules on ice and water interfaces.

Interestingly, the adsorption of methanol and acetone on ice and water surfaces impacts the hydrogen bonded region. The extracted frequencies of the hydrogen bonded O-H stretch modes are illustrated in Figure 4. For the methanol-ice interface, a blue-shift of ~80 cm^{-1} is observed. The blueshift indicates a weakening of the hydrogen bond. The central frequency of the O-H stretch vibration is sensitive to both the strength and arrangement of the hydrogen bond.[33] The strength of a hydrogen bond, which depends on the intermolecular distance between the hydrogen and oxygen and the angles of the acceptor orientation weakens the covalent O-H bond in the donor molecule. This weakening results in a lower O-H stretch vibrational frequency. As a result, the shift in the O-H stretch frequency induced by hydrogen bonding can be directly related to the energy of the hydrogen bond. Here, we observe a blueshift of the O-H frequency, which is indicative of a decrease in the hydrogen bond strength. This is in contrast to the acetone adsorption, where the observed redshift is ~10 cm^{-1}, as illustrated in Figure 4b and in previous literature.[32] This clearly demonstrates that short chain alcohols, such as methanol, adsorbs on ice surface completely different than the carbonyl group containing organic pollutants, such as acetone. The contrasting shift in the bonded O-H stretch mode upon adding acetone or methanol to ice surfaces can significantly influence vibrational overtone pumping reactions. The frequency difference of the O-H stretch mode for methanol on ice versus acetone on ice is over 100 cm^{-1}. Here, we are monitoring the O-H fundamental frequency. The overtone frequency is roughly double the frequency of the fundamental, which could result in drastically different photochemical reactions on ice surfaces for these small organic molecules.

Overtone transitions that are excited in the near-IR and visible regions are primarily driven by stretching overtones of C-H, O-H, S-H or N-H. Consequently, the O-H stretching overtone of water molecules of the C-H stretching overtone of methanol molecules may give rise to different vibrational overtone chemistry when triggered by sunlight. These processes could help resolve discrepancies between atmospheric models and measurements. Vaida and Donaldson[34] reviewed the unimolecular chemistry of atmospheric compounds containing OH groups, such as hydrogen peroxide and pyruvic acid. Although the dissociation of alcohols occurs at frequencies outside the range of solar radiation, the fundamental insights of water mediated vibrational overtone reactions is important owing to the ability of water molecules to form hydrogen bonds with oxidized species.[35–37]

For methanol on the surface of ice, the blue shift or weakening of the hydrogen bonds is indicative of surface melting. The premelted liquid layer on ice, also known as the quasi-liquid layer (QLL), influences a wide range of geophysical and atmospheric phenomena.[38,39] Previously the QLL on ice surfaces was measured with SFG spectroscopy and it was determined that the surface premelting occurs in bilayers. Sánchez et al.[22] determined the surface melting by a blue shift in the hydrogen bonded region, similar to the spectra of illustrated here. Thus, our data suggests that methanol adsorbed onto the ice surface is forming a liquid-like layer, composed of water molecules and methanol molecules, on the surface of ice.

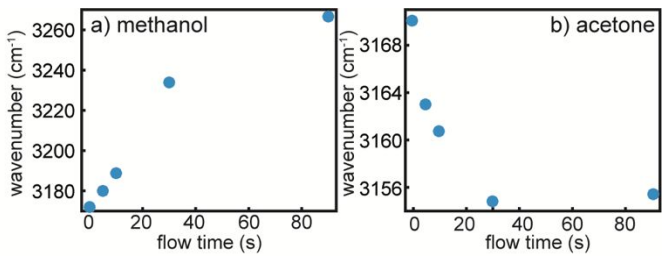

Figure 4. Extracted peak positions from the fits of the SFG spectra for a) methanol and b) acetone on ice surfaces.

To further understand the different mode of adsorption of methanol on water compared to carbonyl containing organic pollutants, we also carried out SFG measurements in the free O-H or dangling O-H region. The representative spectrum for methanol-water interface in the free O-H region is shown in Figure 5. The amplitude of the free O-H group does not significantly change with the addition of methanol on water surfaces. Previous SFG studies by Schaefer et al.[30] have illustrated SFG spectra of pure methanol that have no free O-H peak.

The adsorption of methanol contrasts with the adsorption of acetone on aqueous interface. In case of acetone, the amplitude of free O-H decreases with the addition of acetone, while new spectral feature arises at 3600 cm^{-1}, converting free O-H groups into O-H groups hydrogen bonded to carbonyl group of acetone molecules.[32] The results here indicate that methanol molecules are not hydrogen bonding to the free O-H groups of water, rendering the interaction between acetone and aqueous interfaces stronger than interactions with methanol and aqueous interfaces. The free O-H signal in the spectra in Figure 5 may also arise in part from the methanol molecules themselves. In order to understand the contribution and surface layer composition isotopically label experiments will be completed in the future. Regardless, the molecular level interactions of acetone and methanol with the dangling O-H groups on water and ice surfaces is significantly different. Our data suggests that the bonding of methanol to the hydroxyls at the water surface are weaker than acetone. This could have implications towards the ability for molecules to "stick" to water or ice surfaces or to transport more readily to other surfaces.

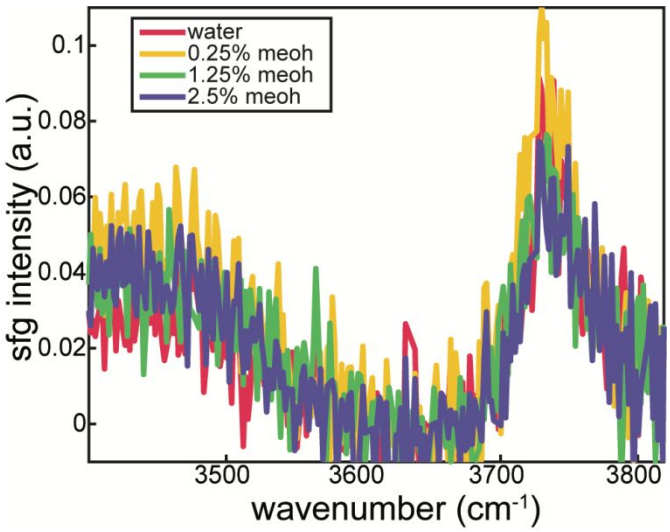

Figure 5. SFG spectra of methanol on water surfaces in the free OH spectral region.

Conclusions

In this study of the adsorption of trace gases on ice and water surfaces, we have shown distinct differences in the behaviour of water molecules with the adsorption of methanol and acetone utilizing surface specific SFG spectroscopy. The adsorption of methanol on ice surfaces weakens the hydrogen bonds and melts the surface of ice. Acetone adsorbed onto ice surfaces red shifts the hydrogen bond O-H frequency. The opposing shift of the fundamental O-H stretching vibration is significant, which could lead to changes in overtone pumping reactions on aqueous surfaces. The adsorption of methanol on water surfaces does not significantly alter the free O-H vibrations. These results illustrate that small carbonyl molecules and small alcohols (hydroxyl molecules) have marked differences on ice surfaces, which can influence the fate of small organic molecules in the atmosphere.

Future studies on photodissocation of organic molecules on ice surfaces would afford the ability to investigate the reaction rates at interfaces to gain more insights on the fate and transport of organic compounds. In previous studies, fluorescence-based techniques were used to estimate the photodissociation rates of simple organic molecules at various interfaces and found that reaction rates are enhanced at ice surfaces compared to aqueous interface.[40,41] The molecular level details extracted from time-resolved SFG spectroscopy would provide key insights on the enhancement of reactions on ice surfaces.

Author contributions

The conception and design of this study were carried out by G.R.Y. and J.D.C. All authors contributed to the experiments, data acquisition, analysis and interpretation and drafting of the manuscript.

Conflicts of interest

There are no conflicts to declare.

Data availability

Data are available upon request from authors. The python code used to fit the SFG data can be found at https://github.com/BoiseState-Chem/SFG_Fit.

Acknowledgements

We thank Joe McCulloch and Marc-Jan van Zadel for excellent technical support. We thank Lindsey D. Jenkins and Oliviero Andressui for improving the python code for SFG fitting and Lila J. Towers for helpful discussions and training. This work was funded by the Welch Foundation (Grant No. AA-2029-20200401) and the National Science Foundation (Grant 2314913). Student support (L.B.M.) was provided by the Idaho Space Grant Consortium, a NASA funded program under Federal Award 80NSSC20M0108. The content of this manuscript is solely the responsibility of the authors and does not necessarily represent the official views of the funding agencies.

Notes and references

1 D. J. Donaldson, G. J. Frost, K. H. Rosenlof, A. F. Tuck and V. Vaida, *Geophys. Res. Lett.*, 1997, **24**, 2651–2654.
2 M. D. Likar, A. Sinha, T. M. Ticich, R. L. Vander Wal and F. F. Crim, *Berichte Bunsenges. Für Phys. Chem.*, 1988, **92**, 289–295.
3 A. Sinha, R. L. Vander Wal and F. F. Crim, *J. Chem. Phys.*, 1989, **91**, 2929–2938.
4 M. G. Lawrence and P. J. Crutzen, *Tellus B Chem. Phys. Meteorol.*, 1998, **50**, 263–289.
5 C. Voigt, B. Kärcher, H. Schlager, C. Schiller, M. Krämer, M. de Reus, H. Vössing, S. Borrmann and V. Mitev, *Atmospheric Chem. Phys.*, 2007, **7**, 3373–3383.
6 F. Dominé and P. B. Shepson, *Science*, 2002, **297**, 1506–1510.
7 A. M. Grannas, A. R. Bausch and K. M. Mahanna, *J. Phys. Chem. A*, 2007, **111**, 11043–11049.
8 L. Jaeglé, D. J. Jacob, W. H. Brune, I. Faloona, D. Tan, B. G. Heikes, Y. Kondo, G. W. Sachse, B. Anderson, G. L. Gregory, H. B. Singh, R. Pueschel, G. Ferry, D. R. Blake and R. E. Shetter, *J. Geophys. Res. Atmospheres*, **105**, 3877–3892.
9 H. Singh, Y. Chen, A. Staudt, D. Jacob, D. Blake, B. Heikes and J. Snow, *Nature*, 2001, **410**, 1078–1081.
10 D. Ardura, T. F. Kahan and D. J. Donaldson, *J. Phys. Chem. A*, 2009, **113**, 7353–7359.
11 J. E. Schaff and J. T. Roberts, *Langmuir*, 1998, **14**, 1478–1486.
12 P. Behr, A. Terziyski and R. Zellner, *J. Phys. Chem. A*, 2006, **110**, 8098–8107.
13 A. K. Winkler, N. S. Holmes and J. N. Crowley, *Phys. Chem. Chem. Phys.*, 2002, **4**, 5270–5275.
14 M. P. Bernstein, J. P. Dworkin, S. A. Sandford and L. J. Allamandola, *Meteorit. Planet. Sci.*, 2001, **36**, 351–358.
15 D. E. Starr, D. Pan, J. T. Newberg, M. Ammann, E. G. Wang, A. Michaelides and H. Bluhm, *Phys. Chem. Chem. Phys.*, 2011, **13**, 19988–19996.
16 J. T. Newberg and H. Bluhm, *Phys. Chem. Chem. Phys.*, 2015, **17**, 23554–23558.
17 P. Jedlovszky, G. Hantal, K. Neuróhr, S. Picaud, P. N. M. Hoang, P. von Hessberg and J. N. Crowley, *J. Phys. Chem. C*, 2008, **112**, 8976–8987.
18 F. Dominé and L. Rey-Hanot, *Geophys. Res. Lett.*, 2002, **29**, 20-1-20–4.
19 K. D. Gibson, G. G. Langlois, W. Li, D. R. Killelea and S. J. Sibener, *J. Chem. Phys.*, 2014, **141**, 18C514.
20 M. J. Shultz, A. Brumberg, P. J. Bisson and R. Shultz, *Proc. Natl. Acad. Sci.*, 2015, **112**, E6096–E6100.
21 X. Wei, P. B. Miranda and Y. R. Shen, *Phys. Rev. Lett.*, 2001, **86**, 1554–1557.
22 M. A. Sánchez, T. Kling, T. Ishiyama, M.-J. van Zadel, P. J. Bisson, M. Mezger, M. N. Jochum, J. D. Cyran, W. J. Smit, H. J. Bakker, M. J. Shultz, A. Morita, D. Donadio, Y. Nagata, M. Bonn and E. H. G. Backus, *Proc. Natl. Acad. Sci.*, 2017, **114**, 227–232.
23 P. Sudera, J. D. Cyran, M. Bonn and E. H. G. Backus, *J. Phys. Chem. C*, 2021, **125**, 22937–22942.
24 Y. Nojima, Y. Suzuki, M. Takahashi and S. Yamaguchi, *J. Phys. Chem. Lett.*, 2017, **8**, 5031–5034.
25 W. J. Smit, J. Versluis, E. H. G. Backus, M. Bonn and H. J. Bakker, *J. Phys. Chem. Lett.*, 2018, **9**, 1290–1294.
26 T. Ishiyama and A. Morita, *J. Phys. Chem. C*, 2007, **111**, 721–737.
27 T. Ishiyama and A. Morita, *J. Phys. Chem. C*, 2007, **111**, 738–748.
28 H. Chen, W. Gan, B. Wu, D. Wu, Y. Guo and H. Wang, *J. Phys. Chem. B*, 2005, **109**, 8053–8063.
29 H. Chen, W. Gan, R. Lu, Y. Guo and H. Wang, *J. Phys. Chem. B*, 2005, **109**, 8064–8075.
30 J. Schaefer, E. H. G. Backus, Y. Nagata and M. Bonn, *J. Phys. Chem. Lett.*, 2016, **7**, 4591–4595.
31 J. Sung, K. Park and D. Kim, *J. Phys. Chem. B*, 2005, **109**, 18507–18514.
32 J. D. Cyran, E. H. G. Backus, M.-J. van Zadel and M. Bonn, *Angew. Chem. Int. Ed.*, 2019, **58**, 3620–3624.
33 R. Rey, K. B. Møller and J. T. Hynes, *J. Phys. Chem. A*, 2002, **106**, 11993–11996.
34 V. Vaida and D. J. Donaldson, *Phys. Chem. Chem. Phys.*, 2014, **16**, 827–836.
35 F. F. Crim, *Proc. Natl. Acad. Sci.*, 2008, **105**, 12654–12661.
36 M. Staikova and D. J. Donaldson, *Phys. Chem. Earth Part C Sol. Terr. Planet. Sci.*, 2001, **26**, 473–478.
37 D. J. Donaldson and D. Anderson, *J. Phys. Chem. A*, 1999, **103**, 871–876.
38 J. G. Dash, A. W. Rempel and J. S. Wettlaufer, *Rev. Mod. Phys.*, 2006, **78**, 695–741.
39 T. Bartels-Rausch, H.-W. Jacobi, T. F. Kahan, J. L. Thomas, E. S. Thomson, J. P. D. Abbatt, M. Ammann, J. R. Blackford, H. Bluhm, C. Boxe, F. Domine, M. M. Frey, I. Gladich, M. I. Guzmán, D. Heger, Th. Huthwelker, P. Klán, W. F. Kuhs, M. H. Kuo, S. Maus, S. G. Moussa, V. F. McNeill, J. T. Newberg, J. B. C. Pettersson, M. Roeselová and J. R. Sodeau, *Atmos Chem Phys*, 2014, **14**, 1587–1633.
40 T. F. Kahan and D. J. Donaldson, *J. Phys. Chem. A*, 2007, **111**, 1277–1285.
41 T. F. Kahan and D. J. Donaldson, *Environ. Sci. Technol.*, 2010, **44**, 3819–3824.

Data availability

Data are available upon request from authors. The python code used to fit the SFG data can be found at https://github.com/BoiseState-Chem/SFG_Fit.